Comparison of straight and curved-ray surface wave tomography at near-surface scale A 3d numerical example

Karimpour, M.; Slob, E.; Socco, L. V.

DOI
10.3997/2214-4609.202210595

Publication date
2022

Document Version
Final published version

Published in
83rd EAGE Conference and Exhibition 2022

2022 EAGE ANNUAL
83RD CONFERENCE & EXHIBITION
MADRID I SPAIN

COMPARISON OF STRAIGHT AND CURVED-RAY SURFACE WAVE TOMOGRAPHY AT NEAR-SURFACE SCALE: A 3D NUMERICAL EXAMPLE

M. Karimpour[1], E. Slob[2], L.V. Socco[1]

[1] Politecnico Di Torino; [2] Delft University of Technology

Summary

Surface Wave Tomography (SWT) is used to build shear-wave velocity models. In some studies, it is assumed that surface waves propagation follows a straight line between the source and the receiver. This assumption might be violated in near-surface studies because of high level of complexity and lateral heterogeneity. In curved-ray SWT, the actual ray paths between every receiver couple are computed. Curved-ray SWT can increase the accuracy of the model and will increase the computational effort. It is important to investigate the gained model improvement together with the associated additional computational cost from curved-ray over straight-ray SWT for near-surface applications. We apply straight- and curved-ray SWT on a generated 3D synthetic dataset and compare the results in terms of accuracy and computational costs

Comparison of straight and curved-ray surface wave tomography at near-surface scale: A 3D numerical example

Introduction

Surface waves are widely analysed to obtain shear-wave velocity (VS) models and surface wave tomography (SWT) is a method that has provided valuable information about the Earth's crust and mantle in seismological studies. In SWT, the dispersion information between receiver pairs is processed to obtain path-averaged slowness dispersion curves (DCs). To build VS models, the estimated DCs are used to build phase (or group) velocity maps at different periods. The velocity maps are then inverted to produce VS models. Alternatively, the VS models can be obtained by direct inversion of DCs avoiding the construction of the phase velocity maps.
Since recently, SWT has increasingly attracted the attention of researchers in near-surface studies (e.g., Rector et al., 2015; Ikeda and Tsuji, 2020) because of its ability to provide high lateral resolution. In some of the SWT near-surface studies it is assumed that surface waves propagate along a straight line between the source and the receiver, which is the traditional assumption in seismology. However, this assumption might not be valid due to the high level of complexity and lateral heterogeneity in near-surface structures. To address this issue, curved-ray SWT can be used where the actual ray path of each frequency component of the DC is computed. This can increase the accuracy of the final model and will increase the computational cost. Having an estimation of the computational cost plays an important role in near-surface studies since the abundance of the available data can increase the computational effort drastically. Therefore, it seems important to investigate the gained model improvement together with the associated additional computational cost from curved-ray over straight-ray SWT for near-surface applications.
We first explain the applied methodology. We then apply straight- and curved-ray SWT on a generated 3D synthetic dataset. The obtained models from the two approaches are depicted and the accuracy of the final models as well as the computational costs are compared.

Method

The input data for SWT are DCs. In this work, the path-average slowness dispersion data between each receiver pair aligned with a source are computed using an automatic picking code (Papadopoulou, 2021). In curved-ray SWT, first the actual ray path between the receiver pair for each frequency component of the DC is computed. Then the forward response (i.e., simulated DCs) is computed as:

$$p_{R_1R_2}(f) = \frac{\int_{l_{R_1R_2}} p(f,l)\,dl}{\int_{l_{R_1R_2}} dl} \quad (1),$$

where $p_{R_1R_2}(f)$ represents the frequency dependent average phase slowness between the receiver pair (R_1 and R_2), and $l_{R_1R_2}$ is the computed ray path between the receiver couple. The ray paths between each receiver pair, which correspond to the least traveltimes, are computed by solving the eikonal equation using a finite-difference scheme (Noble et al., 2014). In case of straight-ray SWT, all ray paths between the receiver couple are pre-defined as straight lines.
The applied inversion algorithm is based on the method proposed by Boiero (2009). To solve the inverse problem, we aim to minimize the misfit function in the least squares sense. The misfit function, Q, is defined as:

$$Q = \left[\left(\mathbf{d}_{obs} - g(\mathbf{m})\right)^T \mathbf{C}_{obs}^{-1}\left(\mathbf{d}_{obs} - g(\mathbf{m})\right)\right] + \left[\left(\mathbf{R_p m}\right)^T \mathbf{C}_{\mathbf{R_p}}^{-1}\left(\mathbf{R_p m}\right)\right] \quad (2),$$

where $\mathbf{m}$ shows the vector of the model parameters, $\mathbf{d}_{obs}$ is the observed data, $g(\mathbf{m})$ represents the vector of forward response of the model, $\mathbf{C_{obs}}$ consists of the uncertainties of the observed data, $\mathbf{R_p}$ is the spatial regularization matrix and $\mathbf{C}_{\mathbf{R_p}}$ represents the covariance of the spatial regularization. The

defined misfit function in eq. (2) is minimised iteratively. At the nth iteration, the current model $\mathbf{m}_n$ is updated as:

$$\mathbf{m}_{n+1} = \mathbf{m}_n + \left(\begin{array}{l} \left[\mathbf{G}^T \mathbf{C}_{obs}^{-1} \mathbf{G} + \mathbf{R}_p^T \mathbf{C}_{R_p}^{-1} \mathbf{R}_p + \lambda \mathbf{I} \right]^{-1} \\ \times \left[\mathbf{G}^T \mathbf{C}_{obs}^{-1} \left(\mathbf{d}_{obs} - g(\mathbf{m}_n) \right) + \mathbf{R}_p^T \mathbf{C}_{R_p}^{-1} \left(-\mathbf{R}_p \mathbf{m}_n \right) \right] \end{array} \right) \quad (3),$$

where $\mathbf{G}$ is the sensitivity matrix of the data and λ represents the damping factor.

Numerical Example

The synthetic data were generated using a 3D- finite difference code (Bohlen et al., 2016). The source emits a 40 Hz Ricker wavelet. To avoid numerical dispersion, the minimum element size is defined such that at least 8 grid-points are present for the shortest wavelength to model the elastic waves propagation. To respect the wavelength sampling criteria a mesh with element size of 0.1 m (in horizontal and vertical dimensions) was defined. To ensure the stability of the simulation, the time stepping was set to 1.0e-6 s to satisfy Courant-Friedrichs-Lewy time stability condition.
The true model consists of a sequence of layers with vertically increasing velocity values, surrounding two velocity anomalies which extend 4 m in horizontal and vertical directions (Figure 1). Receivers are located with a 1 m spacing in an area of 20 m × 20 m (Figure 1a). In total, 971 DCs were estimated.

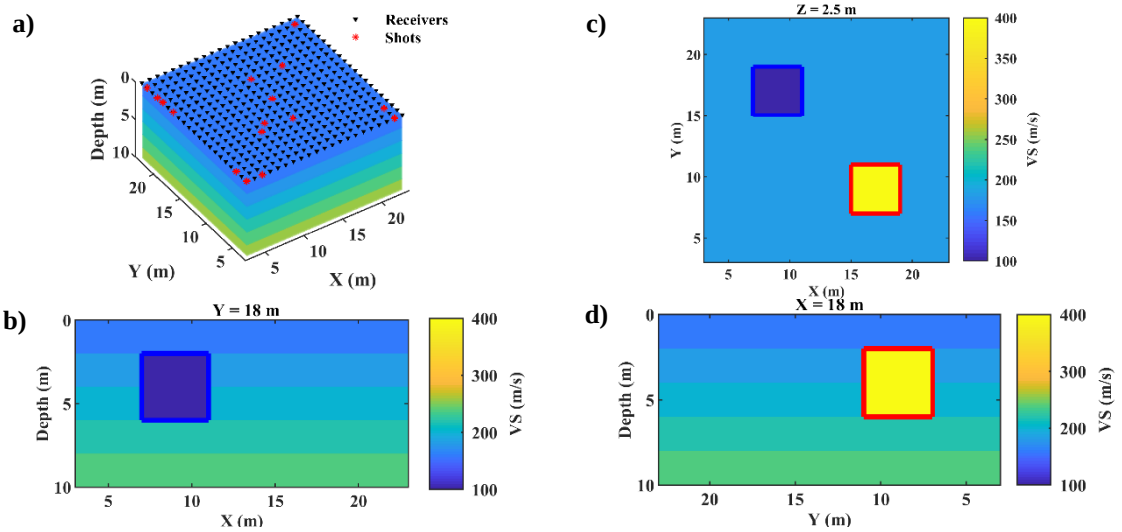

Figure 1*. True VS model. a) 3D view of the model together with the acquisition geometry, b) vertical slice at Y = 18 m, c) horizontal slice at 2.5 m depth, d) vertical slice at X=18m. The boundaries of the low- and high-velocity anomalies are superimposed in blue and red, respectively.*

The initial model for the inversion is defined as a 5-layer 3D model where the thickness of each layer is fixed at 2 m. The horizontal dimensions of each inversion block are 2m on the side and have an initial constant VS value of 200 m/s. The Poisson ratio and density values are assumed to be known as a priori information and are equal to 0.33 and 2000 kg/m^3 in the whole subsurface. The geophysical properties of the true and initial models are reported in Table 1 and Table 2. The same initial model is used as the starting model for the SWT inversion in both straight- and curved-ray methods. The inversion results are displayed in Figure 2.

Table 1. *Parameters of the True Model*

Layer	VS (m/s)	ν (-)	h (m)	ρ (kg/m^3)
1	160	0.33	2	2000
2	100-400	0.33	2	2000
3	100-400	0.33	2	2000
4	220	0.33	2	2000
5	240	0.33	2	2000

Table 2 *Geophysical parameters of the initial model*

Layer	VS (m/s)	ν (-)	h (m)	ρ (kg/m^3)
1	200	0.33	2	2000
2	200	0.33	2	2000
3	200	0.33	2	2000
4	200	0.33	2	2000
5	200	0.33	2	2000

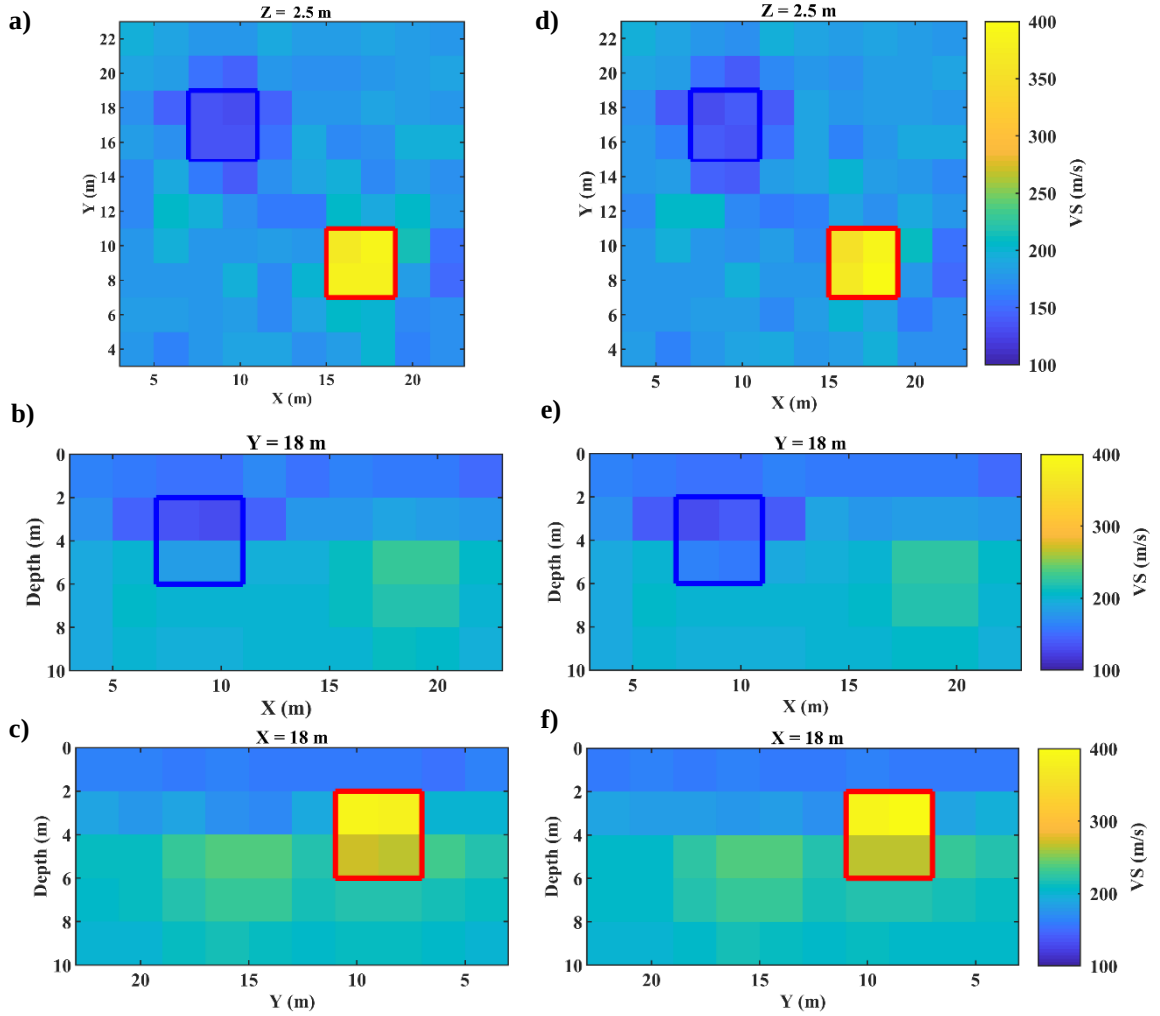

***Figure 2**. SWT inversion results. Straight-ray SWT results are shown at: a) 2.5 m depth, b) Y = 18 m, c) X = 18 m, and the results of the curved-ray for the same slices are displayed at d-f.*

Figure 2 shows that straight- and curved-ray SWT have modelled the location and the value of the high-velocity anomaly quite accurately. The model from the curved-ray method is slightly superior at the grid blocks surrounding the high-velocity box (Figures 2d and 2f). In case of low-velocity anomaly, curved-ray SWT has provided better results, because the bottom half of the low velocity box is better resolved by the curved-ray approach (Figure 2e). Examples of the computed ray paths by curved-ray SWT in vicinity of the velocity anomalies are illustrated in Figure 3.

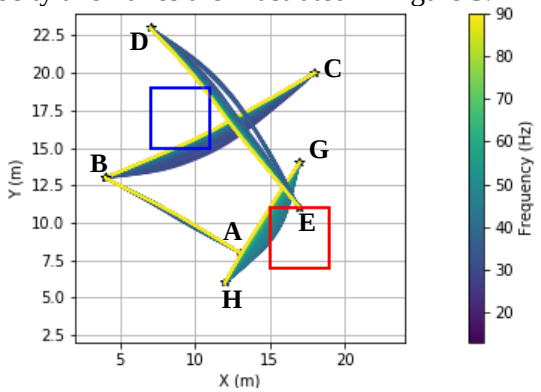

***Figure 3**. Examples of ray paths of the DCs in curved-ray SWT. The receivers are labelled as A-H. The boundaries of the low- and high-velocity anomalies are superimposed in blue and red, respectively.*

Figure 3 depicts intriguing results having in mind that the inversion process started from a completely homogeneous VS model. The computed ray paths between receivers A and B in Figure 3 show that in case of smooth lateral heterogeneity, the curved-ray SWT produces the same results as straight-ray SWT. However, the paths between G and H in Figure 3 clarify that the high-velocity portion causes deviation from the straight line. It can also be seen that the deviation increases as the frequency decreases, with almost zero deviation from the straight-line for the frequency components that travel in depths shallower than the top of the anomaly (2m). The displayed ray paths between B and C, and between D and E in Figure 3, show the superiority of the curved-ray approach at the interface of the low-velocity anomaly as the lower frequency components of the DCs tend to travel through the faster portion, bypassing the low velocity volume. The model accuracy and computational cost of the straight- and curved-ray methods are compared quantitatively in Table 3.

Table 3*. Quantitative comparison of straight- and curved-ray SWT.*

Type of SWT	Average final data misfit (%)	Average final model misfit (%)	Run time (hours)	Peak memory-consumption (GB)
Straight-ray	0.98	10.9	2	2.85
Curved-ray	0.98	10.76	6.1	3.85

We see in Table 3 that the curved-ray method has slightly decreased the final model misfit at the cost of tripling the computational effort. Even though the final model misfit is slightly lower (0.14 %) in the curved-ray approach, not only the run time has increased, also the memory has increased with 35 %.

Conclusions

We have shown that SWT is a powerful tool to build VS models at near-surface scale in presence of high lateral heterogeneity. In our 3D numerical example, straight-ray and curved-ray SWT have produced similar final models. The obtained model from curved-ray SWT has improved the accuracy, particularly at modelling the low-velocity anomaly in the vertical direction. However, it has considerably increased the computational cost.

Acknowledgements

We would like to thank Compagnia di San Paolo for funding the PhD scholarship of Mohammadkarim Karimpour.

References

Bohlen, T., and F. Wittkamp, 2016, Three-dimensional viscoelastic time-domain finite-difference seismic modelling using the staggered Adams–Bashforth time integrator, Geophysical Journal International, 204(3), 1781–1788.

Boiero, D., 2009, Surface wave analysis for building shear wave velocity models: PhD thesis, Politecnico di Torino.

Ikeda, T., and Takeshi Tsuji, 2020, Two-station continuous wavelet transform cross-coherence analysis for surface-wave tomography using active-source seismic data, Geophysics, 85, EN17-EN28.

Papadopoulou, M., 2021, Surface wave methods for mineral exploration: Ph.D. thesis, Politecnico di Torino.

Rector, J. W., J. Pfeiffe, S. Hodges, J. Kingman, and E. Sprott, 2015, Tomographic imaging of surface waves: A case study from the Phoenix Mine, Battle Mountain, Nevada, The Leading Edge, 34(11), 1360-1364.

Noble, M., A., Gesret, and N., Belayouni, 2014, Accurate 3-D finite difference computation of traveltimes in strongly heterogeneous media, Geophysical Journal International, 199(3), 1572-1585.